THE JOURNAL OF PHYSICAL CHEMISTRY LETTERS
A JOURNAL OF THE AMERICAN CHEMICAL SOCIETY

pubs.acs.org/JPCL

Letter

Crystal Structure of Symmetric Ice X in H_2O-H_2 and H_2O–He under Pressure

Jialin Lei, Jinhyuk Lim, Minseob Kim, and Choong-Shik Yoo*

Cite This: *J. Phys. Chem. Lett.* 2021, 12, 4707–4712

Read Online

ACCESS | Metrics & More | Article Recommendations | Supporting Information

ABSTRACT: Ice VII and ice X are the two most dominant phases, stable over a large pressure range between 2 and 150 GPa and made of fundamentally different chemical bonding. Yet, the two ice phases share a similar bcc-based crystal structure and lattice constants, resulting in a challenge to discern the crystal structure of ice VII and ice X. Here, we present well-resolved X-ray diffraction data of H_2O in quasi-hydrostatic H_2 and He pressure media, clearly resolving the two ice phases to 130 GPa and the dissociative nature of ice VII to X transition occurring at 20–50 GPa in H_2O-H_2 and 60–70 GPa in H_2O–He. The present diffraction data permits, for the first time, the accurate determination of the bulk moduli B_0 of 225 (or 228) GPa for ice X and 6.2 (or 4.5) GPa for ice VII, in H_2O-H_2 (or H_2O–He), which can provide new constraints for Giant planetary models.

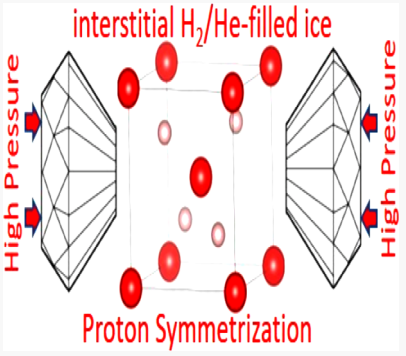

Water as the most common molecule containing hydrogen bonds exhibits remarkable phase polymorphism over a wide range of thermodynamic conditions.[1−6] The relatively weak hydrogen bonding (with respect to covalent −OH bonds and other covalent bonds) is often subjected to large distortions in the bond angle and topology, resulting in a myriad of phases—both stable and metastable in crystalline and amorphous phases. Over 15 phases of ices have been identified to date, and most of them were discovered below 2 GPa.[7−11] Despite the rich polymorphs at low pressures, only two ice phases are known over a wide range of pressures between 2 and 150 GPa at ambient temperature; proton disordered ice VII[12] and symmetrically ordered ice X[13,14] for which the proton locates at the midpoint between two neighboring oxygen atoms. Above 150 GPa, additional phases have been suggested, both theoretically[15,16] and experimentally,[14] in which the bcc sublattice in ice X undergoes a possible transformation to an antifluorite-like or a hexagonal close packed (hcp) structure. Further compression will eventually close the bandgap of these materials (i.e., metallic-ice).[17] With increasing temperature above 40–100 GPa, *ab initio* molecular dynamics (MD) simulations have found an evidence for enhanced hydrogen self-diffusion, leading to significant ionic conductivity below the melting curves of H_2O and NH_3 (i.e., superionic states[18,19]). Several superionic states of H_2O have also been predicted in H_2O–He even at lower pressures.[20]

Ice VII and ice X are two most fundamental ice polymorphs, stable over a large pressure region between 2 and 150 GPa and made of characteristic inter- and intramolecular hydrogen bonding networks. Yet, they share a similar bcc-based crystal structure and lattice constants; for example, the overall structure of ice VII can be described as two interpenetrating hydrogen-bond networks. With increasing pressure, the nearest neighbor oxygen–oxygen distance in ice VII decreases and eventually brings all hydrogen atoms at the midway points of the neighboring oxygen atoms in ice X with symmetrized −O–H–O− bonds. As such, the transition between the two accompanies a continuous change in hydrogen bonding, bond distance, and strength, occurring over a large pressure range, 40–80 GPa.[12,14]

Because of the similarity in crystal structure, it has been challenging to discern the crystal structure of ice X from ice VII, and the onset of transition between the two. The structures of ice VII and X can be characterized by examining the translational motion of protons. Recent neutron diffraction data,[21,22] for example, indicated a dissociative structural transition to interstitial filled ice VII at 11 GPa, with the elongation of covalent O–H bonds, at a rate of which rapidly increases with pressure, into a distinct regime of ice X. Still neutron data are available only for ice VII within a limited pressure range below 60 GPa,[21,22] insufficient to understand the structure and properties of ice X and the exact nature of the ice VII-to-X transition. On the other hand, it is very difficult to resolve the two phases by X-ray diffraction, because not only do the X-rays primarily probe oxygen atoms in very similar bcc

Received: February 24, 2021
Accepted: May 10, 2021
Published: May 12, 2021

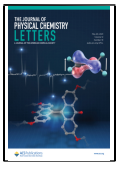

https://doi.org/10.1021/acs.jpclett.1c00606
J. Phys. Chem. Lett. 2021, 12, 4707–4712

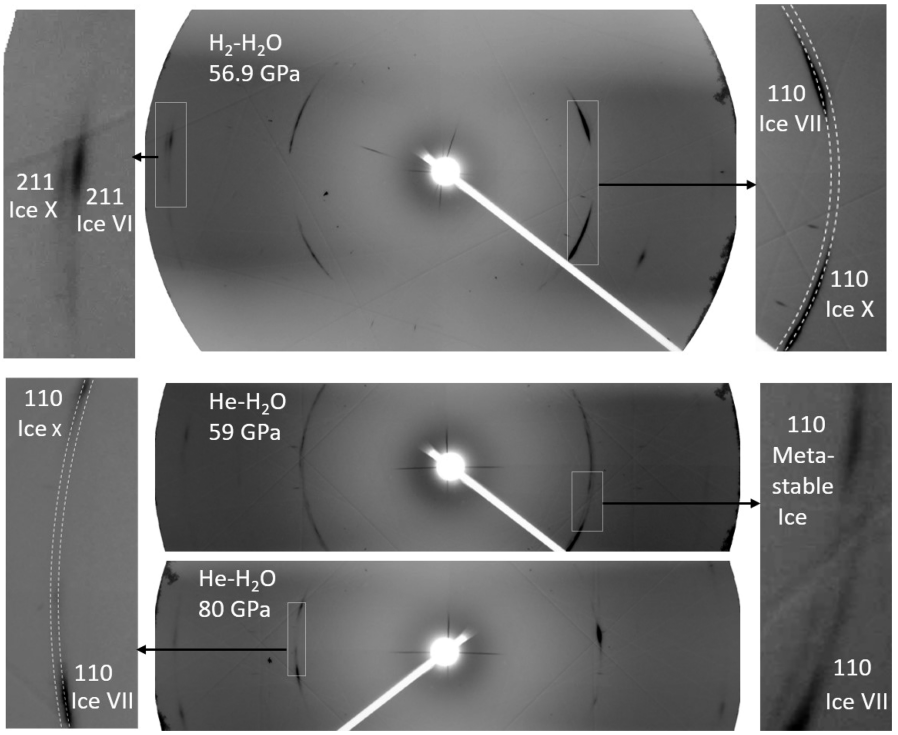

Figure 1. Two-dimensional diffraction images of H_2O−H_2 and H_2O−He at high pressures. Debye−Scherrer diffraction rings as recorded on MAR CCD, showing the evidence for peak splitting of the (111) and (211) of ice VII. The dashed lines are guides for the eyes.

sublattices but also strong nonhydrostaticity develops in hydrogen bonded ice phases at high pressures that result in broadening of the diffraction lines. As a result, the structure and properties of ice X have not been measured directly but are based on the approximation and extrapolation of those of ice VII.

In this study, we report new angle-dispersive X-ray diffraction (ADXD) data of both ice X and ice VII obtained in quasi-hydrostatic pressure media H_2 and He to 130 GPa. The data show a set of clearly resolved diffraction lines of ice VII and ice X and, thereby, provides new structural information on ice X, for the first time, and critical constraints for the EOS of ice X and also VII, as well as the transition between the two.

The experiments were performed using diamond anvil cells (DAC) with beveled diamond anvils (Type Ia) with a typical culet size of 100 μm in diameter. Rhenium gaskets were preindented to ∼30 μm in thickness, and small holes of ∼80 μm in diameter were drilled at the center using an electric discharge machine. Deionized H_2O was loaded in the DAC, followed by loading high-pressure gas of He or H_2 at around 2000 atm using a home-built high-pressure gas loader. A small piece of Cu chip was also loaded as a pressure calibrant.[23] *In situ* angle-dispersive X-ray diffraction experiments were carried out at the 16IDB/HPCAT beamline at the Advanced Photon Source (APS), using microfocused (3 μm × 6 μm in beam size) monochromatic X-rays (0.4066 Å) and MAR CCD detector. We used a standard CeO_2 powder to determine the sample-to-detector distance, the X-ray beam center, and the detector tilt. The 2D diffraction images of samples were recorded on the detector, integrated with DIOPTAS,[24] then analyzed using XRDA.[25]

Two-dimensional diffraction images of H_2O in H_2 and He consist of discontinuous Debye−Scherrer diffraction rings (Figure 1). Yet, the splittings in several diffraction rings are unambiguously observed to discern the emergence of ice X from ice VII to ∼130 GPa—the maximum pressure studied. Note that the H_2O sample was loaded in a liquid form, and it crystallizes when pressure is applied. Therefore, it is difficult to control the crystallite size and grain number statistics, especially of a small sample in a beveled DAC. The fair degree of peak broadening observed could be attributed to the dramatic change in stiffness when ice VII transformed to ice X or change in crystallite size with increasing pressure. At low pressures, the diffraction data of H_2O in H_2 (Figure 2a) show evidence for the formation of hydrogen clathrate hydrate at ∼7 GPa, which can be indexed to a cubic structure with a space group of $Fd3m$. This is consistent with the early reported ice hydrate $C2$ structure,[26,27] where oxygen atoms adopt a diamond-like lattice with guest hydrogen molecules sitting in the octahedral interstitial sites. The cubic clathrate phase remains observable to ∼30 GPa, above which it breaks down and disappears as expected because the separation into solid H_2 and ice VII is more energetically favorable than maintaining the less effective packing of clathrate phase. All other remaining diffraction peaks including (110), (200), and (211) of ice VII split into two. It clearly indicates the formation of two bcc-like lattices, which can be attributed to ice VII and ice X. This in turn highlights the onset of ice VII to X transition at 30 GPa. Despite the transition, however, the peaks of ice VII remain recognizable to the highest pressure reached in the present experiments.

H_2O in He (Figure 2b) shows no clathrate formation at ambient temperature, as expected. He clathrate hydrates are known to form only at low temperatures below 250 K.[28,29] On the other hand, the diffraction spectra of H_2O in He show an emergence of a new peak (noted by a green star) at the left side of the (110) at 22 GPa, which diminishes at ∼60 GPa.

https://doi.org/10.1021/acs.jpclett.1c00606
J. Phys. Chem. Lett. 2021, 12, 4707−4712

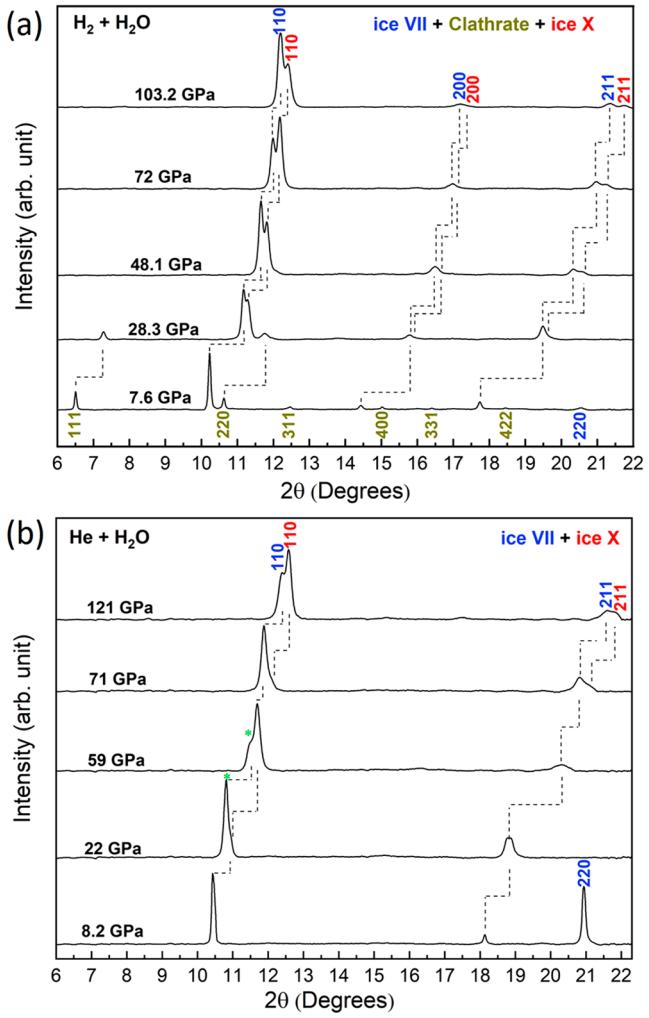

Figure 2. Representative angle dispersive X-ray diffraction patterns of solid H_2O at high pressures using (a) H_2 and (b) He as pressure transmitting medium. Miller indices for different phases observed are included on the plot. The dashed lines help to guide the view for the peak shifting. Green stars indicate a metastable phase previously reported in ref 30.

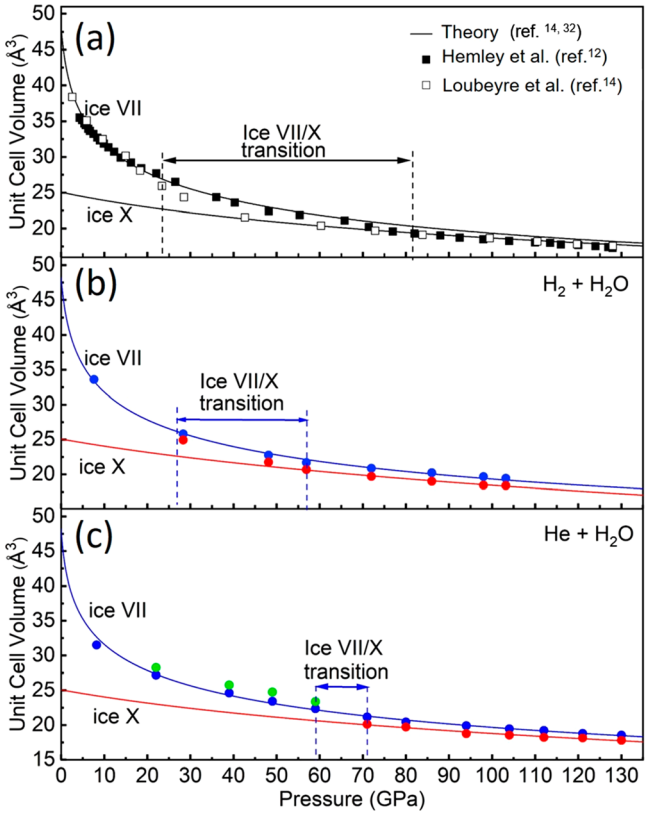

Figure 3. Volume compression data of ice VII (blue), ice X (red), and metastable ice (green) using H_2 and He as pressure transmitting medium, respectively. The experimental and theoretical data are shown in the plot labeled with black (close and open) square and solid lines. Error bars smaller than symbol size are omitted. The volume compression data can be found in the Supporting Information.

This is likely from metastable ice, previously observed in pure H_2O at ~14 GPa.[30] The crystal structure of the metastable ice remains unsolved because of the paucity of diffraction lines. Here, we index the new peak as (110), assuming a bcc-like ice VII structure. Upon the disappearance of metastable ice, the peaks (110) and (211) from ice X appear on the right sides to the ice VII peaks at 70 GPa. Then, ice VII and ice X in H_2O–He coexist over a large pressure range to ~130 GPa, as observed in H_2O–H_2.

Figure 3 plots the specific volumes of ice VII and X phases measured in H_2O–H_2 and H_2O–He in the present study (also see Supplementary Table S1), in comparison with those of pure ice VII previously measured[12,14] and ice X previously calculated.[31,32] The previous compression data of pure ice VII (closed[12] and open[14] circles in Figure 4a) follow the calculated ones (black lines), initially of ice VII and then ice X, underscoring a continuous transition from ice VII to ice X over a large pressure region of 25 to 80 GPa. As a result, the equation of state (EOS) fit of ice VII, for example, represents that of mixed ice VII and X, while that of ice X is only known from the theoretical calculations. The present compression data obtained in H_2O–H_2 (Figure 3b) and H_2O–He (Figure 3c), on the other hand, is clearly distinguishable for ice VII (blue circles and lines) and ice X (red circles and lines), providing critical constraints for the untainted structure properties of the two phases, for the first time.

The pressure–volume compression data of H_2O–H_2 and H_2O–He are fitted to the third-order Birch–Murnaghan equation-of-state (BM-EOS)[33] with the ambient volume V_o of 48.22 Å^3 and 25.06 Å^3 for ice VII[14] and ice X,[32] respectively. The resulting bulk modulus B_0 and its pressure derivative B' are summarized in Table 1: in H_2O–H_2, B_0 (B') = 6.2 (6.9) GPa for ice VII, and 227.8 (2.6) GPa for ice X. In H_2O–He, B_0 (B') = 4.5 (8.7) GPa for ice VII, and 224.9 (3.1) GPa for ice X. Using a different value for V_0 of 25.57 Å^3,[31] the bulk modulus becomes 192.7 GPa—still substantially larger than that of ice VII, which underscores the nature of covalent network of ice X. These values are in good agreement with those previously calculated B_0 (B') = 5.9 (7.1) GPa for ice VII and 198 (3.7) GPa for ice X.[31,32] The present values for ice VII are, as expected, considerably lower than that previously measured from powder X-ray diffraction, B_0 = 14.9–24.6 GPa,[12,34−37] but is in good agreement with that previously measured from single crystal X-ray diffraction of pure ice VII, B_0 = 4.26 GPa.[14] Note that no experimental value has been reported for ice X previously.

High bulk modulus of ice X clearly indicates the extended (or polymeric) nature of its structure made of a covalent –O–

https://doi.org/10.1021/acs.jpclett.1c00606
J. Phys. Chem. Lett. 2021, 12, 4707−4712

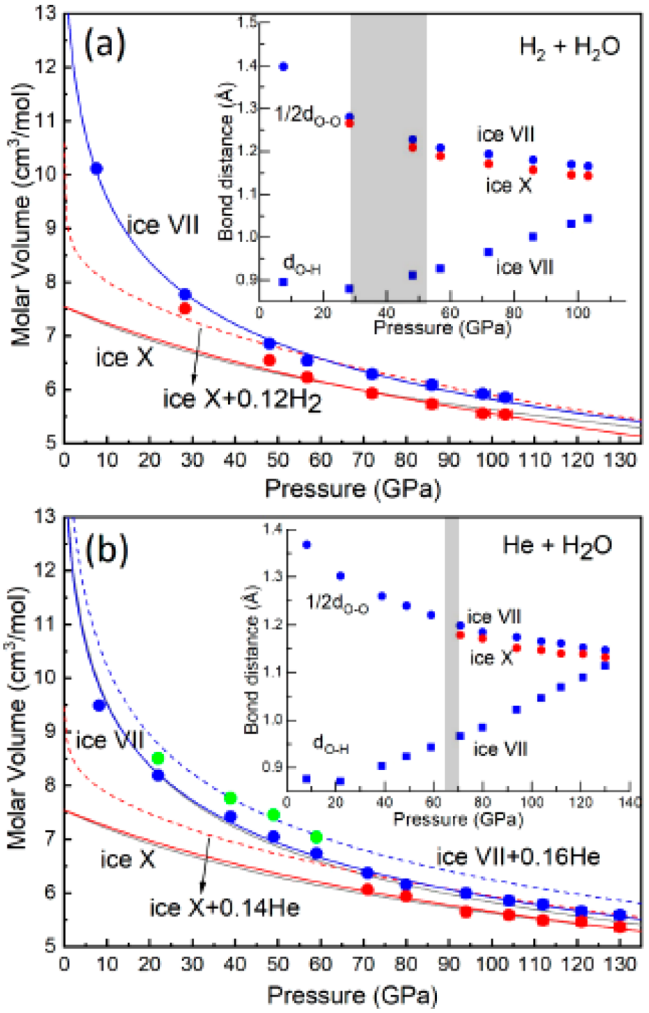

Figure 4. Equations of state of gas-filled ice phases calculated using EOS of H_2O and literature EOS of pure He and H_2. The theoretical EOS of H_2O was plotted in gray. The insets show the evolution of the bond distance of O−H and O−O upon compression.

Table 1. Birch−Murnaghan Equation of State of Ice VII and Ice X in Comparison

phases	B_0 (GPa)	B'	V_0 (Å^3)	refs
ice VII in H_2O−H_2	6.2 (±0.9)	6.9 (±0.7)	48.22[b]	this study
ice VII in H_2O−He	4.5 (±1.0)	8.7 (±1.7)	48.22[b]	this study
pure ice VII	14.9−24.6; 4.25[a]			34−37,12, and 14
theoretical	5.9	7.1		31
ice X in H_2O−H_2	227.8 (±14.7)	2.6 (±0.3)	25.06[c]	this study
	194.6 (±11.0)	3.0 (±0.3)	25.57[d]	this study
ice X in H_2O−He	224.9 (±22.0)	3.1 (±0.5)	25.06[c]	this study
	192.7 (±20.0)	3.4 (±0.5)	25.57[d]	this study
theoretical	198	3.7		32

[a]Reference 14 for single crystal ice VII. [b]Reference 14. [c]Reference 32. [d]Reference 31.

H−O− network structure, which is subjected to a large differential stress and a significant pressure gradient at high pressures. Such a nonhydrostatic condition develops as ice VII transforms to ice X. This makes it difficult to resolve the diffraction lines between the two phases and, in turn, explains a surprisingly large difference in the transition pressure previously reported; for example, the lower bound of the transition ranges from 25 GPa[14] to 65 GPa,[12] whereas the upper bound ranges from 70 GPa[13,38,39] to 110 GPa.[22] The broad transition pressure in pure ice then compares with the relatively sharp transitions in H_2O−H_2 and H_2O−He in particular, occurring within considerably smaller pressure ranges of 20−55 GPa and 60−70 GPa, respectively. When ice VII transforms to ice X, its bulk modulus increases significantly from ∼5 GPa to ∼200 GPa. In the case of nonhydrostatic compression, the microstrain supported by the lattice of stiff ice X under high pressure can cause a remarkable peak broadening and this combined with the great pressure gradient in the sample chamber can make the peak splitting shown in Figure 2 hardly detected, resulting in a broad transition window in pressure as shown in Figure 3. In the case of quasi-hydrostatic compression, the soft He and H_2 can mitigate the pressure gradient and peak broadening; therefore, it allows for a better diffraction resolution to observe the phase transition and yields a sharper transition. It is also important to note a substantially lower transition pressure observed in H_2O−H_2 than in H_2O−He or pure H_2O. This is consistent with the previous Raman results in D_2−H_2O,[40] where the interstitial filled D_2 increases the local electron density of H_2O,[41] creating a large internal chemical pressure (i.e., $P = -(\delta E/\delta V)_T$) and thereby lowering the transition pressure to 20−50 GPa. On the other hand, such an effect is small for He with filled $1s^2$ orbital in H_2O−He and become important only when the temperature is lower than 250 K[29] and pressure higher than 300 GPa.[42] Therefore, the transition occurs relatively sharply at ∼70 GPa—a considerably higher pressure than that in H_2O−H_2, but nearly the same as the upper bound transition pressure of pure H_2O.[13,38,39]

It is remarkable to note in H_2O−H_2 (Figure 3b) and H_2O−He (Figure 3c) that ice VII and ice X coexist over the entire pressure range studied (to 130 GPa). This is contrary to pure H_2O (Figure 3a), where ice VII simply disappears or smoothly converts to ice X. The coexistence of ice VII and ice X in H_2O−H_2 or H_2O−He is likely due to the inclusion of H_2 or He in the ice phases, which can enhance the stability entropically (i.e., $-T\Delta S$) well beyond those of pure phases. To evaluate the inclusion model, we compare the molar volumes of ice VII and ice X with those of interstitial H_2 (or He)-filled ice phases, as shown in Figure 4. The molar volume of ice VII in H_2−H_2O (a) and He−H_2O (b) above ∼70 GPa is in fact in excellent agreement with the 12% H_2- or 14% He-filled pure ice X. This translates into an interstitial occupancy of 0.5 protons (or 0.3 He), in agreement with the previously reported 0.2−1.0.[21] In turn, the present model seems to support the observation of metastable ice phase (green circles in Figure 4b) to be 0.16 He-filled ice VII.

The present structure data provide insights into the dissociative nature of phase VII-to-X transition and proton symmetrization. The insets in Figure 4 plot the O−H intramolecular bond distance (d_{O-H}) and the O−O intermolecular bond distance (d_{O-O}) as a function of pressure. In ice X, the proton distribution function statistically maximizes at the center of the O−O bond distance (i.e., $d_{O-H} = {}^1/_2 d_{O-O}$). Here, the proton position of ice VII has been determined by the previous neutron diffraction data[21] and then

https://doi.org/10.1021/acs.jpclett.1c00606
J. Phys. Chem. Lett. 2021, 12, 4707−4712

extrapolated to higher pressures employing a linear regression fit (see Supplementary Figure S1 and Table S2). The insets clearly show a continuous elongation of d_{O-H}, while decreasing d_{O-O}, with increasing pressure. It clearly indicates a dissociative nature of the transition from ice VII to ice X, which occurs over a broad pressure range in H_2O-H_2 at 30−55 GPa, but relatively sharply in H_2O−He at ∼70 GPa.[43,44] Considering nearly nonbonding interaction between He and H_2O, the onset of the ice VII to ice X transition is most likely at ∼70 GPa or d_{O-H} = 0.96 Å, accompanying a 5.7% volume collapse. The observed volume change is strongly dependent on the transition pressure, consistent with that predicted from theoretical calculations (see the gray lines in Figure 4). This compares with $^1/_2 d_{O-O}$ = 1.18 Å of ice X at the transition, signifying an abrupt nature of the first-order phase transition. The same transition in H_2O-H_2, on the other hand, occurs progressively at substantially shorter O−H distances between d_{O-H} = 0.88 and 0.94 Å, highlighting the presence of internal chemical pressure of interstitial filled H_2.

In summary, we presented angle dispersive X-ray diffraction data of H_2O in H_2O-H_2 and H_2O−He to ∼130 GPa. Because of the quasi-hydrostatic conditions of H_2 and He, the diffraction lines of ice VII and ice X were clearly discerned, providing for new constraints for crystal structure and EOS of ice X and ice VII, as well as the dissociative structural transition between the two occurring at 20−50 GPa in H_2O-H_2 and 60−70 in H_2O−He. The present diffraction data permits, *for the first time*, the accurate determination of the bulk moduli B_0 of 225 (or 228) GPa for ice X and 6.2 (or 4.5) GPa for ice VII, in H_2O-H_2 (or H_2O−He), which provide new constraints for chemical bonding in ice phases and Giant planetary models.[46,47] The high bulk modulus value of ice X is consistent with the recent observation by Mendez et al. in dynamic-DAC experiments.[48] The results also show evidence for the presence of ice VII well into the stability region of ice X, which can be considered as the interstitial H_2- or He-filled ice X.

Finally, the present results of H_2O−He and H_2O-H_2 are important for understanding the miscibility of H_2 and He in dense ices and solid-state host−guest chemistries. The results also have significant implications to high-pressure research using H_2 or He as a quasi-hydrostatic pressure medium and modeling the internal structure, composition, and properties of Giant planets,[45,48] especially for the boundary region of the upper H_2−He layer and the middle "ice" layers. The incorporation of He and H_2 in dense ice driven by an increasing entropy, for example, can have significant effects on the ionic conductivity and diffusivity of ice[47,20] and, thereby the dynamo and convection of the fluid ice layer.

■ ASSOCIATED CONTENT

Supporting Information

The Supporting Information is available free of charge at https://pubs.acs.org/doi/10.1021/acs.jpclett.1c00606.

Pressure−volume data for ice VII and ice X measured in H_2O-H_2 and H_2O−He; structural parameters of ice VII used to calculate the neutron diffraction pattern; pressure-dependent changes of the (110)/(220) ratio and order parameter of ice VII (PDF)

■ AUTHOR INFORMATION

Corresponding Author

Choong-Shik Yoo − *Institute of Shock Physics and Department of Chemistry, Washington State University, Pullman, Washington 99164, United States;* orcid.org/0000-0002-2664-0730; Email: csyoo@wsu.edu

Authors

Jialin Lei − *Institute of Shock Physics and Department of Chemistry, Washington State University, Pullman, Washington 99164, United States*

Jinhyuk Lim − *Institute of Shock Physics and Department of Chemistry, Washington State University, Pullman, Washington 99164, United States*

Minseob Kim − *Institute of Shock Physics and Department of Chemistry, Washington State University, Pullman, Washington 99164, United States*

Complete contact information is available at: https://pubs.acs.org/10.1021/acs.jpclett.1c00606

Notes

The authors declare no competing financial interest.

■ ACKNOWLEDGMENTS

The X-ray work has been performed at 16IDB/HPCAT at the APS. We acknowledge the effort of Yue Meng and Curtis Kenney-Benson for their assistance at the beamline. Funding: We acknowledge funding from the NSF (DMR 1701360), DOE-NNSA (DE-NA0003342) and ARO (W911NF-17-1-0468). Portions of this work were performed at HPCAT (Sector 16), Advanced Photon Source (APS), Argonne National Laboratory. HPCAT operations are supported by DOE-NNSA's Office of Experimental Sciences. The Advanced Photon Source is a U.S. Department of Energy (DOE) Office of Science User Facility operated for the DOE Office of Science by Argonne National Laboratory under Contract No. DE-AC02-06CH11357.

■ REFERENCES

(1) Mishima, O.; Stanley, H. E. The Relationship between Liquid, Supercooled and Glassy Water. *Nature (London, U. K.)* **1998**, *396*, 329−335.

(2) Ohmine, I.; Saito, S. Water Dynamics: Fluctuation, Relaxation, and Chemical Reactions in Hydrogen Bond Network Rearrangement. *Acc. Chem. Res.* **1999**, *32*, 741−749.

(3) Poirier, J. P. Rheology of Ices: A Key to The Tectonics of The Ice Moons of Jupiter and Saturn. *Nature (London, U. K.)* **1982**, *299*, 683−687.

(4) Klug, D. D. Dense Ice in Detail. *Nature (London, U. K.)* **2002**, *420*, 749−751.

(5) Yoshimura, Y.; Stewart, S. T.; Somayazulu, M.; Mao, H.-K.; Hemley, R. J. High-Pressure X-Ray Diffraction and Raman Spectroscopy of Ice VIII. *J. Chem. Phys.* **2006**, *124*, 024502.

(6) Sugimura, E.; Komabayashi, T.; Ohta, K.; Hirose, K.; Ohishi, Y.; Dubrovinsky, L. S. Experimental Evidence of Superionic Conduction in H_2O Ice. *J. Chem. Phys.* **2012**, *137*, 194505.

(7) Hemley, R. J. Effects of High Pressure on Molecules. *Annu. Rev. Phys. Chem.* **2000**, *51*, 763−800.

(8) Chen, J. Y.; Yoo, C. S. High Density Amorphous Ice at Room Temperature. *Proc. Natl. Acad. Sci. U. S. A.* **2011**, *108*, 7685−7688.

(9) Finney, J. L.; Bowron, D. T.; Soper, A. K.; Loerting, T.; Mayer, E.; Hallbruker, A. Structure of A New Dense Amorphous Ice. *Phys. Rev. Lett.* **2002**, *89*, 205503.

(10) Tulk, C. A.; Benmore, C. J.; Urquidi, J.; Klug, D. D.; Neufeind, J.; Tomberli, B.; Enelstaff, P. A. Structural Studies of Several Distinct Metastable Forms of Amorphous Ice. *Science* **2002**, *297*, 1320−1323.
(11) Salzmann, C. G.; Radaelli, P. D.; Hallbrucker, A.; Mayer, E.; Finney, J. L. The Preparation and Structures of Hydrogen Ordered Phases of Ice. *Science* **2006**, *311*, 1758−1761.
(12) Hemley, R. J.; Jephcoat, A. P.; Mao, H.-K.; Zha, C. S.; Finger, L. W.; Cox, D. E. Static Compression of H_2O-Ice to 128 GPa (1.28 Mbar). *Nature (London, U. K.)* **1987**, *330*, 737−740.
(13) Goncharov, A. F.; Struzhkin, V. V.; Somayazulu, M. S.; Hemley, R. J.; Mao, H.-K. Compression of Ice to 210 Gigapascals: Infrared Evidence for A Symmetric Hydrogen-Bonded Phase. *Science* **1996**, *273*, 218−220.
(14) Loubeyre, P.; Letoullec, R.; Wolanin, E.; Hanfland, M.; Häusermann, D. Modulated Phases and Proton Centering in Ice Observed by X-Ray Diffraction up to 170gpa. *Nature (London, U. K.)* **1999**, *397*, 503−506.
(15) Wang, Y.; Liu, H.; Lv, J.; Zhu, L.; Wang, H.; Ma, Y. High Pressure Partially Ionic Phase of Water Ice. *Nat. Commun.* **2011**, *2*, 563.
(16) Pickard, C. J.; Martinez-Canales, M. Decomposition and Terapascal Phases of Water Ice. *Phys. Rev. Lett.* **2013**, *110*, 245701.
(17) Hermann, A.; Ashcroft, N. W.; Hoffmann, R. High Pressure Ices. *Proc. Natl. Acad. Sci. U. S. A.* **2012**, *109*, 745−750.
(18) Cavazzoni, C.; Chiarotti, G. L.; Scandolo, S.; Tosatti, E.; Bernasconi, M.; Parrinello, M. Superionic and Metallic States of Water and Ammonia at Giant Planet Conditions. *Science* **1999**, *283*, 44−46.
(19) Millot, M.; Coppari, F.; Rygg, J. R.; Barrios, A. C.; Hamel, S.; Swift, D. C.; Eggert, J. H. Nanosecond X-Ray Diffraction of Shock-Compressed Superionic Water Ice. *Nature (London, U. K.)* **2019**, *569*, 251−255.
(20) Liu, C.; Gao, H.; Wang, Y.; Needs, R. J.; Pickard, C. J.; Sun, J.; Wang, H. T.; Xing, D. Multiple Superionic States in Helium−Water Compounds. *Nat. Phys.* **2019**, *15*, 1065−1070.
(21) Guthrie, M.; Boehler, R.; Tulk, C. A.; Molaison, J. J.; dos Santos, A. M.; Li, K.; Hemley, R. J. Neutron Diffraction Observations of Interstitial Protons in Dense Ice. *Proc. Natl. Acad. Sci. U. S. A.* **2013**, *110*, 10552−10556.
(22) Guthrie, M.; Boehler, R.; Molaison, J. J.; Haberl, B.; dos Santos, A. M.; Tulk, C. Structure and Disorder in Ice VII on The Approach to Hydrogen-Bond Symmetrization. *Phys. Rev. B: Condens. Matter Mater. Phys.* **2019**, *99*, 184112.
(23) Dewaele, A.; Loubeyre, P.; Mezouar, M. Equations of State of Six Metals above 94 GPa. *Phys. Rev. B: Condens. Matter Mater. Phys.* **2004**, *70*, 094112.
(24) Prescher, C.; Prakapenka, V. B. *DIOPTAS*: A Program for Reduction of Two-Dimensional X-Ray Diffraction Data and Data Exploration. *High Pressure Res.* **2015**, *35*, 223−230.
(25) Desgreniers, S.; Lagarec, K. *XRDA*3.1 - A Program for X-Ray Diffraction Analysis on A PC. *J. Appl. Crystallogr.* **1998**, *31*, 109−110.
(26) Vos, W. L.; Finger, L. W.; Hemley, R. J.; Mao, H. K. Novel H_2-H_2O Clathrates at High Pressures. *Phys. Rev. Lett.* **1993**, *71*, 3150−3153.
(27) Vos, W. L.; Finger, L. W.; Hemley, R. J.; Mao, H. K. Pressure Dependence of Hydrogen Bonding in A Novel H_2O-H_2 Clathrate. *Chem. Phys. Lett.* **1996**, *257*, 524−530.
(28) Londono, D.; Kuhs, W. F.; Finney, J. L. Enclathration of Helium in Ice II: The First Helium Hydrate. *Nature (London, U. K.)* **1988**, *332*, 141−142.
(29) Kuhs, W. F.; Hansen, T. C.; Falenty, A. Filling Ices with Helium and The Formation of Helium Clathrate Hydrate. *J. Phys. Chem. Lett.* **2018**, *9*, 3194−3198.
(30) Somayazulu, M.; Shu, J.; Zha, C. S.; Goncharov, A. F.; Tschauner, O.; Mao, H.-K.; Hemley, R. J. *in situ* High-Pressure X-Ray Diffraction Study of H_2O Ice VII. *J. Chem. Phys.* **2008**, *128*, 064510.
(31) Sugimura, E.; Iitaka, T.; Hirose, K.; Kawamura, K.; Sata, N.; Ohishi, Y. Compression of H_2O Ice to 126 GPa and Implications for Hydrogen-Bond Symmetrization: Synchrotron X-Ray Diffraction Measurements and Density-Functional Calculations. *Phys. Rev. B: Condens. Matter Mater. Phys.* **2008**, *77*, 214103.
(32) Caracas, R. Dynamical Instabilities of Ice X. *Phys. Rev. Lett.* **2008**, *101*, 085502.
(33) Birch, F. Finite Strain Isotherm and Velocities for Single-Crystal and Polycrystalline NaCl at High Pressures And 300 K. *J. Geophys. Res.* **1978**, *83*, 1257−1268.
(34) Liu, L. Compression of Ice VII to 500 Kbar. *Earth Planet. Sci. Lett.* **1982**, *61*, 359−364.
(35) Fei, Y. W.; Mao, H. K.; Hemley, R. J. Thermal Expansivity, Bulk Modulus, and Melting Curve Of H_2O−Ice VII To 20 GPa. *J. Chem. Phys.* **1993**, *99*, 5369−5373.
(36) Wolanin, E.; Pruzan, P.; Chervin, J. C.; Canny, B.; Gauthier, M.; Hausermann, D.; Hanfland, M. Equation of State of Ice VII up to 106 GPa. *Phys. Rev. B: Condens. Matter Mater. Phys.* **1997**, *56*, 5781−5785.
(37) Frank, M. R.; Fei, Y. W.; Hu, J. Z. Constraining the Equation of State of Fluid H_2O to 80 GPa Using The Melting Curve, Bulk Modulus, and Thermal Expansivity of Ice VII. *Geochim. Cosmochim. Acta* **2004**, *68*, 2781−2790.
(38) Aoki, K.; Yamawaki, H.; Sakashita, M.; Fujihisa, H. Infrared Absorption Study of The Hydrogen-Bond Symmetrization in Ice to 110 GPa. *Phys. Rev. B: Condens. Matter Mater. Phys.* **1996**, *54*, 15673−15677.
(39) Ahart, M.; Somayazulu, M.; Gramsch, S. A.; Boehler, R.; Mao, H. K.; Hemley, R. J. Brillouin Scattering of H_2O Ice to Megabar Pressures. *J. Chem. Phys.* **2011**, *134*, 124517.
(40) Borstad, G. M.; Yoo, C. S. H_2O And D_2 Mixtures under Pressure: Spectroscopy and Proton Exchange Kinetics. *J. Chem. Phys.* **2011**, *135*, 174508.
(41) Ashcroft, N. W. Hydrogen Dominant Metallic Alloys: High Temperature Superconductors. *Phys. Rev. Lett.* **2004**, *92*, 187002.
(42) Liu, H.; Yao, Y.; Klug, D. D. Stable Structures of He and H_2O at High Pressure. *Phys. Rev. B: Condens. Matter Mater. Phys.* **2015**, *91*, 014102.
(43) Ji, C.; Li, B.; Liu, W.; Smith, J. S.; Majumdar, A.; Luo, W.; Ahuja, R.; Shu, J.; Wang, J.; Sinogeikin, S.; Meng, Y.; Prakapenka, V. B.; Greenberg, E.; Xu, R.; Huang, X.; Yang, W.; Shen, G.; Mao, W. L.; Mao, H.-K. Ultrahigh-Pressure Isostructural Electronic Transitions in Hydrogen. *Nature (London, U. K.)* **2019**, *573*, 558−562.
(44) Loubeyre, P.; LeToullec, R.; Pinceaux, J. P.; Mao, H. K.; Hu, J.; Hemley, R. J. Equation of State and Phase Diagram of Solid ^{4}He from Single-Crystal X-Ray Diffraction over A Large *P-T* Domain. *Phys. Rev. Lett.* **1993**, *71*, 2272−2275.
(45) Guillot, T. Interiors of Giant Planets Inside and Outside The Solar System. *Science* **1999**, *286*, 72−77.
(46) Hubbard, W. B.; Burrows, A.; Lunine, J. I. Theory of Giant Planets. *Annu. Rev. Astron. Astrophys.* **2002**, *40*, 103−136.
(47) Salpeter, E. E. On Convection and Gravitational Layering in Jupiter and in Stars of Low Mass. *Astrophys. J.* **1973**, *181*, L83−L86.
(48) Mendez, A. S. J.; Trybel, F.; Husband, R. J.; Steinle-Neumann, G.; Liermann, H. P.; Manquardt, H. Bulk Modulus of H2O across the Ice VII − ice X Transition Measured by Time-Resolved X-ray Diffraction in Dynamic Diamond Anvil Cell Experiments. *Phys. Rev. B: Condens. Matter Mater. Phys.* **2021**, *103*, 064104.

https://doi.org/10.1021/acs.jpclett.1c00606
J. Phys. Chem. Lett. 2021, 12, 4707−4712